Journal of Materials Chemistry C

Solution-Processed Broadband Photodetectors Without Transparent Conductive Oxide Electrodes

Journal:	*Journal of Materials Chemistry C*
Manuscript ID	TC-ART-09-2021-004278.R1
Article Type:	Paper
Date Submitted by the Author:	26-Oct-2021
Complete List of Authors:	Shen, Lening; The University of Akron Yi, Chao; University of Akron, Zheng, Luyao; University of Akron Liu, Yanghe; University of Akron Zheng, Jie; University of Akron, Chemical and Biomolecular Engineering Gong, Xiong; The University of Akron, Polymer Eng

Solution-Processed Broadband Photodetectors Without Transparent Conductive Oxide Electrodes

Lening Sheng,[#,1] Chao Yi,[#,1] Luyao Zheng,[#,1] Yanghe Liu,[1] Jie Zheng,[2] and Xiong Gong*[,1]

1)School of Polymer Science and Polymer Engineering, 2) Department of Chemical, Biomolecular and Corrosion Engineering, College of Engineering and Polymer Science, The University of Akron, Akron, OH 44325

Abstract

Broadband photodetectors (PDs) have great applications in both industrial and scientific sectors. In this study, solution-processed broadband PDs with an "inverted" vertical photodiode device structure without incorporated with the transparent conductive oxides electrodes, fabricated by bulk heterojunction (BHJ) composites composed of a low optical gap conjugated polymer blended with high electrical conductive PbS quantum dots (QDs), operated at room temperature, are reported. The low optical gap conjugated polymer incorporated with PbS QDs contributes to the spectral response from the ultraviolet (UV)-visible to infrared (IR) range. To realize IR spectral response and circumvent the weak IR transparency of the transparent oxides electrodes, implementation of a photodiode with an "inverted" vertical device structure with the Au anode and the Ba/Al bilayer semitransparent cathode passivated with MgF_2 layer is demonstrated. Photo-induced charge carrier transfer occurred within the BHJ composite gave rise to decent photocurrent, resulting in the detectivities greater than 10^{12} Jones (cm $Hz^{1/2}$/W) over the wavelength from the UV-visible to IR range under low applied bias. Thus, our findings of the utilization of the BHJ composites and an "inverted" vertical photodiode without incorporated with the transparent conductive oxides electrodes provide a facile way to realize broadband PDs.

# These authors are contributed to this work equally.

*Corresponding author, email: xgong@uakron.edu, Fax: (330) 972 3406

1. Introduction

Broadband photodetectors (PDs) have drawn great attention in both academic and industrial sectors due to their various applications including telecommunications, day/night surveillance, thermal imaging, chemical/biological sensing, and spectroscopic and medical instruments.[1-4] To realize broadband PDs, currently PDs with different sub-bands were integrated to one electronic device to cover the spectral response from the ultraviolet (UV)-visible to infrared (IR) range.[1-5] Moreover, InCaAs- and HgCdTe-based IR PDs require an extremely low operating temperature (4.2K) and operate at high voltage to achieve reasonable detectivity.[1,2] In addition, expensive manufacturing processes are required to fabricate these IR PDs.[1-3,6] All these requirements restrict their application in biosensors and image sensors where both high sensitivity and low operating voltage are required.[1-3]

In the past years, inorganic quantum dots (QDs) based PDs with a planar device structure have been extensively studied to realize IR responsibility, but high operation voltages were required to achieve a decent detectivity.[4,6-10] Two-dimensional (2D) materials, such as graphene and transition metal dichalcogenides, have been studied as the alternatives to demonstrate IR detection with high detectivities through PDs with the device structure the same as that of thin-film transistors (TFTs).[11-14] However, their applications are restricted by the difficulty in large-scale and high throughput fabrication of mono- and multi-layer 2D materials as well as the high gate (or drive) voltages to be used for TFTs.[11-14] In the past two decades, organic/polymer-based PDs have gained abundant attention due to their advanced features such as ease of processing, low cost, physical flexibility, and excellent optoelectronic properties.[5,15-17] In 2009, we reported polymer-based PDs with spectral response from 300 nm to 1450 nm.[5] Recently, we demonstrated polymer-based PDs with spectral response from 300 nm to 2500 nm.[17] Various novel molecules

were developed for extending the spectral response of polymer-based PDs.[18-21] Furthermore, film morphology evolution,[22] interfacial engineerings,[23,24] molecular engineering and arrangement,[25,26] and the photomulitpication (PM) effect,[27-29] have been used to enhance the detectivities of polymer-based PDs. However, it is still a challenge to realize polymer-based PDs with decent IR photoresponse because of their short exciton lifetime induced by the phonon-exciton recombination[30-34]

To circumvent the above challenges, either polymers or hybrid perovskites incorporated with inorganic QDs have been developed to realize broadband PDs.[4,23,24,35-41] In the past years, we reported various room-temperature (RT) operated broadband PDs by conjugated polymers, inorganic QDs, conjugated polymers incorporated with inorganic QDs, and hybrid perovskites incorporated with inorganic QDs.[4,23,24,35-41]

On the other hand, the transparent electrodes are required to realize PDs with IR spectral response. However, currently widely used transparent conductive oxides, such as indium tin oxide (ITO) and fluorine-doped tin oxide (FTO), as the transparent electrodes for various electronics including sensors and PDs, possess very weak transmittance in the IR region.[42-44] Thus, PDs with a planar device structure and a TFTs device structure were developed to avoid using neither ITO nor FTO electrodes, realizing IR spectral response.[6-14] Furthermore, carbon nanotubes (CNTs),[45,46] silver nanowires (Ag NWs)[47] and semiconducting polymers[48,49,50,51] were under intensive investigation for substitution of ITO or FTO electrodes. But, CNTs and Ag NWs thin films possess poor electrical conductivity[45-49] and were required to be processed with complicated costive nanoimprint lithography as well.[45-49] Semiconducting polymer thin films as the transparent electrodes have drawn much attention owing to their advanced features such as low cost, lightweight, mechanical flexibility, and compatibility with plastic substrates.[50,51] But

semiconducting polymer thin film with high electrical conductivities needs to be treated with strong acids,[50,51] which restrict its practical applications in electronics. Recently, we demonstrated flexible solution-processed broadband PDs with a "vertical" sandwiched device structure, made by hybrid perovskites incorporated with PdSe QDs, based on the solution-processed polymeric thin film as the transparent electrode.[42]

In this study, we report room-temperature (RT) operated solution-processed broadband PDs fabricated by bulk heterojunction (BHJ) composites composed of a low optical gap conjugated polymer blended with high electrical conductive PbS QDs and with an "inverted" vertical photodiode device structure without incorporated with the transparent conductive oxides electrodes. The low optical gap conjugated polymer contributes to the IR photo-response up to 1700 nm. PbS QDs further extend the IR photo-response up to 2000 nm. To realize IR spectral response and circumvent the weak IR transparency of the transparent oxides' electrodes, implementation of a photodiode with an "inverted" vertical device structure with the Au anode and the Ba/Al bilayer semitransparent cathode passivated with MgF_2 layer, is demonstrated. Photo-induced charge carrier transfer occurred within the PDDTT:PbS QDs BHJ composite gave rise to decent photocurrent, resulting in the detectivities greater than 10^{12} Jones (cm $Hz^{1/2}$/W) over the wavelength region from 300 nm to 2000 nm under low applied bias. Thus, our findings of the utilization of the PDDTT:PbS QDs BHJ composites and an "inverted" vertical photodiode without incorporated with the transparent oxides electrodes provide a facile way to realize broadband PDs.

2. Experimental Section

2.1. Materials

PbO (99.999%) was purchased from Alfa Aesar. Oleylamine (OLA) (90%), 1-octadecene (ODE) (90%), trioctylphosphine (TOP) (97%), diphenylphosphine (DPP) (98%) and selenium (99.99%), 1, 2-Ethanedithiol (EDT) (98%), methanol (99.8) and acetonitrile (ACN) (99.8%) were purchased from Sigma Aldrich. All materials are used as received without further purification. The PDDTT was synthesized in our lab followed the procedures reported previosuly.[5]

Synthesis of PbS QDs: $PbCl_2$ (1 mmol, 0.28 g) was added to 5 mL of oleylamine (OLA) at RT, and then heated to 120 ^oC under vacuum and stirred vigorously until the $PbCl_2$-OLA mixture turned into a homogeneous clear solution. Elemental sulfur (0.4 mmol, 14 mg) was dissolved in 2.5 mL of OLA by heating at 80 ^oC in an oil bath, which gave a deep red solution. The resultant sulfur solution was injected into the $PbCl_2$-OLA solution at 140 ^oC, and then kept for 1 hour. The resultant solution was further centrifuged and purified to generate OLA-capped PbS QDs power. The OLA-capped PbS QDs thin film was spin-casted from 50 mg/mL the OLA-capped PbS QDs octane solution, and the cast EDT acetonitrile solution on the top of the OLA-capped PbS QDs. Afterward, acetonitrile solvent is used to wash out the excess organic ligand. Repeat the above steps several times for obtaining the EDT-capped PbS QDs thin film.

2.2. Preparation and characterization of thin films

PDDTT and PbS QDs thin films, and PDDTT:PbS QDs BHJ composite thin film were fabricated through the spin-coat method from their corresponding solutions. Absorption spectra of thin films were measured by Lambda 750 UV/Vis/NIR spectrometer from PerkinElmer Company. The transmission electron microscopy (TEM) images were measured by Model JEOL JSM-1230. The thin film thickness was measured on the DektakXT surface profile system. The transient absorption measurements were carried out using a dual-beam femtosecond spectrometer

utilizing the second harmonic of an OPA (optical parametric amplifier) as the pump and a white light continuum as the probe in Professor Alan J. Heeger's laboratory at the University of California Santa Barbara.

Fabrication and Characterization of TFTs: the ''bottom-contact'' TFTs device structure was treated in hexamethyldisilazane before deposition of PbS QDs thin films. The TFTs device structures with different source-drain separations were fabricated on an n-doped Si wafer; the n-doped Si was used as the gate. The gate dielectric was a 200 nm film of SiO_2 thermally grown directly on the wafer. The source and drain electrodes (Au) were deposited on the SiO_2 by e-beam evaporation. The channel lengths (source-drain separation) was 25 μm, and the channel width was 1000 μm. Electrical measurements were carried out using a Keithley 4200 Semiconductor Characterization System in ambient condition.

2.3. Fabrication and characterization of broadband PDs

Commercially available Au/Cr caped on the glass substrates were cleaned with deionized water, acetone, and isopropanol and then dried out in the vacuum overnight. After UV ozone plasma treatment for 20 minutes (mins) in ambient atmosphere, ~ 30 nm MoO_3 layer was deposited on the top of Au/Cr surface by spin-coat method from MoO_3 precursor solution, followed with thermal annealing at 120 ^oC for 30 mins. ~ 200 nm PDDTT:PbS QDs BHJ composite thin film was spin-coated on the top of MoO_3 layer from PDDTT:PbS QDs BHJ composite toluene solution. After that, a ~ 10 nm BaO, ~ 5 nm Ba, ~ 20 nm Al and ~ 400 nm MgF_2 were thermally deposited consequently through a shadow mask under a vacuum of 1×10^{-6} mbar. The device area was measured to be 0.16 cm^2.

The current density-voltage (J-V) characteristics of broadband PDs were obtained by using a Keithley model 2400 source measurement unit. A Newport Air Mass 1.5 Global (AM1.5G) full-

spectrum solar simulator was applied as the light source. The light intensities for the wavelength (λ) of 800 nm was 0.22 mW cm^{-2} and for λ=1550 nm was 0.05 mW cm^{-2}. The external quantum efficiency (EQE) spectra were measured by a quantum efficiency measurement system (QEX10) with a 300 W steady-state xenon lamp as the source light. The transient photocurrent measurement was performed on a homemade setup by using an optical chopper controlled at λ of 532 nm laser pulse at a frequency of 2 kHz.

3. Results and discussion

To enhance the electrical conductivity of PbS QDs, 1, 2-ethanedithiol (EDT), which is with short thiol (S-H) chain, is used to substitute OLA, which is with long carbon chain (C-C), through the ligand exchange process,[52-55] for generating the EDT-capped PbS QDs (termed as EDT-PbS QDs). After that, the EDT-capped PbS QDs were rinsed with CH_3OH and then treated with $NH_3{\cdot}H_2O$, followed by thermal annealing at 150 ^oC for 10 minutes. The molecular structures of OLA and EDT are shown in **Figure 1a**. The TEM images of the OLA-capped PbS QDs and EDT-capped PbS QDs thin films are presented in **Figure 1b, c**. Based on the TEM image, the average particle size of the OLA-capped PbS QDs is estimated to be ~9 nm; whereas the average particle size of the EDT-capped PbS QDs is estimated to be ~12 nm. Thus, the treatment described above could enlarge the particle size of PbS QDs.

Figure 1d presents the absorption spectra of PbS QDs. The absorption of the OLA-capped PbS QDs is extended to 1900 nm, whereas the absorption of the EDT-capped PbS QDs is extended to 2100 nm. Thus, the optical bandgap (E_g) is estimated to be 0.65 eV for the OLA-capped PbS QDs thin film and 0.59 eV for the EDT-capped PbS QDs thin film. According to the quantum confinement effect,[56] the particle size of the OLA-capped PbS QDs is estimated to be ~

9 nm, whereas the particle size of the EDT-capped PbS QDs is estimated to be ~ 13 nm. These results are in good agreement with the TEM images (**Figure 1b, 1c**).

To verify the hypothesis that the EDT-capped PbS QDs thin film possess superior electronic properties than that of the OLA-capped PbS QDs, the TFTs are applied to study the field-effect mobilities of two different PbS QDs thin films. The field-effect mobility in the saturation regime was extracted using the equation $I_{DS} = C_i\mu (V_{GS} - V_{Th})^2 W/2L$,[57] under the condition of $-V_{DS} > -(V_{GS}-V_{Th})$, where I_{DS} is the source/drain current, μ is the field-effect mobility, W is the channel width, L is the channel length, C_i is the capacitance per unit area of gate dielectric layer, and V_{GS}, V_{Th} and V_{DS} are the gate, threshold, and source/drain voltages, respectively. **Figure 2a** presents I_{DS} vs. V_G characteristics of the TFTs made by two different PbS QDs thin films. The field-effect mobilities of ~ 1 x 10^{-5} $cm^2/V{\cdot}s$ and ~ 2.2 x 10^{-3} $cm^2/V{\cdot}s$ are observed from the OLA-capped PbS QDs thin film and the EDT-capped PbS QDs thin film, respectively. The field-effect hole mobility of the EDT-capped PbS QDs thin film is ~ 100 times larger than that of the OLA-capped PbS QDs thin film. The enhanced charge carrier mobility of the EDT-capped PbS QDs thin film is ascribed to the short-chain of EDT molecule.

Figure 2b compares the dynamics of the photoinduced absorption in the OLA-capped PbS QDs thin film and the EDT-capped PbS QDs thin film probed at 4.7 mm. Compared to the OLA-capped PbS QDs, a fast decay from the EDT-capped PbS QDs thin film was observed. A slow decay indicates that the traps induced by the insulating OLA restrict the electron hopping from one PbS QD to another one. Whereas a fast decay observed from the EDT-capped PbS QDs reveals that the electron can be hopped from one PbS QDs to another with less restriction. These results demonstrate that the charge carrier mobility of the EDT-capped PbS QDs is higher than those of the OLA-capped PbS QDs.

Figure 3a presents the molecular structures of PDDTT with different side chains, where PDDTT is poly(5,7-bis(4-decanyl-2-thienyl)-thieno(3,4-b)diathiazole-thiophene-2,5). PDDTT is selected as the electron donor to form bulk heterojunction (BHJ) composite with PbS QDs since it was a p-type low optical gap conjugated polymer with decent charge carrier mobility.[5] Moreover, PDDTT exhibits optical response up to the near-infrared (NIR) region, which certainly could contribute the NIR spectral response for broadband PDs based on PDDTT composites.[5] However, PDDTT with $C_{10}H_{21}$ side chain (PDDTT-C10) possesses poor solubility in typical organic solvents. To enhance its solubility, a side chain with long carbon, such as $C_{12}H_{25}$ was incorporated with PDDTT. The synthesis procedures of PDDTT with $C_{12}H_{25}$ side chain (PDDTT-C12) were the same as PDDTT-C10, which was reported previously.[5,58] The absorption spectra of PDDTT-C10 and PDDTT-C12 thin films are shown in **Figure 3b.** Due to polymer aggregation,[59] PDDTT-C12 thin film possesses extended absorption compared to PDDTT-C10 thin film. Thus, PDDTT-C12 is used as the electron donor to form a BHJ composite with the EDT-capped PbS QDs for the development of broadband PDs.

Scheme 1a displays the device architecture of the broadband PDs. In this broadband PDs, neither ITO nor FTO, which are currently used as the transparent electrodes for various electronics, are used as the electrodes due to their very weak transmittance in the IR region.[43-45] Moreover, carbon nanotubes (CNTs),[45,46] silver nanowires (Ag NWs)[47] and semiconducting polymers[48,49,50,51] were also not utilized as the transparent electrodes since they possess poor electrical conductivity and are required to be processed with complicated costive nanoimprint lithography.[45-49] Towards the end, an "inverted" device architecture as shown in **Scheme 1a** is developed. In this device structure, the Au/Cr bilayer is as the anode, solution-processed MoO_3 thin layer acts as the hole extraction layer (HEL), the PDDTT:PbS QDs BHJ composite thin film

is the photoactive layer, the vacuum-deposited BaO thin layer acts as the electron extraction layer (EEL), thin Ba covered with Al bilayer acts as the cathode, the transparent MgF_2 layer is used as the passivation layer since it has excellent transparency from the UV-visible to IR region.[60] The Ba/Al (5 nm/20 nm) bilayer has decent transparency from the UV-visible to IR region as well.[61] BaO is a wide optical gap oxide. The light pass through the BaO EEL will be absorbed by the PDDTT:PbS QDs BHJ composite thin film. Moreover, smooth Au layer typical can reflect 30% of light.[62] **Scheme 1b** displays the absorption spectrum of glass Cr/Au thin film. It is clear that smooth Au thin layer could reflect light from 300 nm to 2000 nm. This reflected light can be further reabsorbed by the PDDTT:PbS QDs BHJ composite thin film, resulting in boosted photocurrent. As a result, a decent photocurrent is expected to be observed from the broadband PDs with a device structure shown in **Scheme 1a**.

Scheme 1c displays the lowest unoccupied molecular orbital (LUMO) and the highest occupied molecular orbital (HOMO) energy levels of MoO_3, PDDTT, PbS QDs, BaO, and the work-functions of Au and Ba electrodes. Without illumination, the Schottky barrier formed between the Au anode and the MoO_3 HEL and the Ba cathode and the BaO EEL, could result in suppressed dark current density for broadband PDs. Under illumination, the excitons generated within PDDTT:PbS QDs BHJ composite photoactive layer would dissociate into separated charge carriers under an external electric field created by the work function difference between Au and Ba electrodes. Based on the band alignment, the separated electrons within the PDDTT:PbS QDs BHJ composite could transfer from PDDTT to PbS QDs due to a large LUMO offset between PDDTT and PbS QDs. These separated electrons are further extracted by the BaO HEL, and then collected by the Ba cathode. Meanwhile, the separated holes within PDDTT:PbS QDs BHJ composite could transfer from PbS QDs to PDDTT due to a large HOMOs offset

between PbS QDs and PDDTT. These separated holes are further extracted by the MoO_3 HEL, and then collected by the Au anode. Therefore, broadband PDs with a device structure shown in **Figure 1a** would exhibit boosted R and D*.[5]

To verify the photo-induced charger transfer occured within PDDTT:PbS QDs BHJ composite, the dynamics of the photoinduced absorption in the PDDTT:PbS QDs BHJ composite thin film probed at 4.7 μm is investigated and further compared with those of pristine PDDTT and PbS QDs. The polarons from conjugated polymers could be detected in the mid-IR spectral region.[63-65] As indicated in **Figure 4a**, a fast decay observed from pristine PDDTT thin film indicates that the lifetime of the polarons from PDDTT is very short. A relatively slow decay observed from the EDT-capped PbS QDs indicates that the charge carrier is trapped due to the insulating of the EDT molecule. However, a much longer polaron lifetime, which is up to a nanosecond, is observed from the PDDTT:PbS QD BHJ composite thin film as compared to those from pristine PDDTT thin film and pristine PbS QD thin film. These results reveal that long-lived mobile carriers are with the integration of PDDTT and PbS QDs, and further demonstrate that efficient charge transfer from PDDTT to PbS QDs with inhibited back-transfer. Thus, as expected, broadband PDs based on the PDDTT:PbS QD BHJ composite thin film would exhibit high photocurrent.

The current density versus voltage (J-V) characteristics of broadband PDs operated at RT and measured in dark and under a monochromatic light at a wavelength (λ) of 800 nm with a light intensity of 0.22 mW/cm^2, and at λ of 1550 nm with a light intensity of 0.05 mW/cm^2, are shown in **Figure 4b**. In dark, the broadband PDs exhibit the asymmetric J-V characteristics with the ratification ratio of 2.5 x 10^4 at ± 1 V. These results indicate that the broadband PDs possess excellent photodiode behaviors.[66] Different photocurrent densities observed from the broadband

PDs under different monochromatic light illumination are ascribed to different light intensities, which indicate that the broadband PDs possess different photo-responsibilities.

Responsivity (R) described as $R = J_{ph}/L_{light}$ [5,66] (where J_{ph} is the photocurrent density and L_{light} is the light intensity) is often used to evaluate the device performance of PDs. Under a bias of -0.1 V, R of 73 mA/W and 28.8 mA/W at λ of 800 nm and 1550 nm, respectively, are observed from the broadband PDs. Moreover, under a bias of -0.5 V, R of 545 mA/W and 195 mA/W at λ of 800 nm and 1550 nm, respectively, are observed from the broadband PDs.

If the dark current is only considered as the major contributor to the noise current,[5,36,37] project detectivity (D*) can be described as $D^* = R/\sqrt{2qJ_d}$ [5] (where J_d is the dark current density, q is the elementary electric charge, $q=1.6\times10^{-19}$ C, respectively). Thus, at RT, D* at λ of 800 nm and 1550 nm are calculated to be 1.6 x 10^{13} Jones and 6.4 x 10^{12} Jones (cm $Hz^{1/2}$/W), respectively, for the broadband PDs operated at a bias of -0.1 V. Moreover, at RT and under a bias of -0.5 V, D* at λ of 800 nm and 1550 nm are calculated to be 1.2 x 10^{14} Jones and 4.3 x 10^{13} Jones, respectively, for the broadband PDs. These D* values are compatible with those observed from 2D metal dichalcogenide-based PDs.[11-14] All these results certainly demonstrate that the broadband PDs with a vertical device structure exhibit high R and D*, indicating the broadband PDs have great potential applications.[1-3]

Figure 4c presents the EQE spectrum of the broadband PDs. It is clear that the EQE spectrum of the broadband PDs is the super position of the absorption spectra of the EDT-capped PbS QDs thin film (**Figure 1**), PDDTT thin film (**Figure 3**) and the reflection spectrum of the Au thin layer (**Scheme 1b**).

Based on the EQE spectrum of and D* value at λ of 800 nm and 1550 nm for the broadband PDs, D* values versus wavelength are speculated based on $R = EQE \times \frac{q}{hv} = EQE \times \frac{\lambda}{1240}$. [5,66]

Figure 4c presents D* versus wavelength for the broadband PDs. Under a bias of -0.1 V, the broadband PDs exhibit over 10^{12} Jones from 300 nm to 2000 nm at RT. Such decent D* over the broadband spectral region are ascribed to novel device architecture and the PDDTT:PbS QDs BHJ composite thin film.

The response time is another important parameter used to evaluate the device performance of PDs. **Figure 4d** presents the transient photocurrents of the broadband PDs. The rise time was defined as the time required for output signals to increase from 10% to 90% of saturated photocurrent. Similarly, the fall time was defined as the time required for the output signal to decrease from 90% to 10% of saturated photocurrent.[67,68] A rise time of 11 μs and a fall time of 45 μs are observed from the broadband PDs. Such slow response time is probably originated from the relatively poor electrical conductivity of the EDT-capped PbS QDs thin film.

4. Conclusion

Room-temperature operated, solution-processed broadband photodetectors (PDs) based on low optical gap conjugated polymer incorporated with high electrical conductive PbS quantum dots (QDs) bulk heterojunction (BHJ) composite and inverted photodiode device structure without incorporated with the transparent oxides electrodes, with spectral response ranging from 300 nm to 2000 nm, was demonstrated. The low optical gap conjugated polymer, PDDTT, contributes to the IR photo-response up to 1700 nm. PbS QDs further extend the IR photo-response up to 2000 nm. Implementation of a photodiode with an "inverted" vertical device structure with the Au anode and the Ba/Al bilayer semitransparent cathode passivated with MgF_2 layer realize IR spectral response and circumvent weak IR transparency of the transparent oxides' electrodes. Photo-induced charge carrier transfer occurred within the PDDTT:PbS QDs BHJ composite gave rise to the photocurrent, resulting in the detectivities greater than 10^{12} Jones (cm

$Hz^{1/2}/W$) over the wavelength region from 300 nm to 2000 nm under low applied bias. Thus, our findings of the utilization of PDDTT:PbS QDs BHJ composites and an "inverted" vertical photodiode without incorporated with the transparent oxides electrodes provide a facile way to realize broadband PDs.

Acknowledgments

This contribution is dedicated to celebrating the 80th birthday of Professor Daoben Zhu, a great respectful scientist. We acknowledge National Science Foundation (EECS 1351785) for financial support. We also thank Professor Alan J. Heeger and his group for conducting ultrafast spectroscopy.

References

1) A. Rogalski, Material considerations for third generation infrared photon detectors, *Infrared Phys. Technol.,* **2007**, *50,* 240-252.
2) A. R. Jha, A. Jha, D. A. Jha, IR technology: applications to electrooptics, photonic devices, and sensors, Wiley, New York, 2000.
3) A. Rogalski, HgCdTe IR detector material: history, status and outlook, *Rep. Prog. Phys.,* **2005**, *68*, 2267-2336.
4) C. Liu, K. Wang, P. Du, E. Wang, X. Gong, A. J. Heeger, Ultrasensitive solution-processed broad-band photodetectors using $CH_3NH_3PbI_3$ perovskite hybrids and PbS quantum dots as light harvesters, *Nanoscale*, **2015**, *7*, 16460-16469.

5) X. Gong, M. Tong, Y. Xia, W. Cai, J. S. Moon, Y. Cao, G. Yu, C.-L. Shieh, B. Nilsson, A. J. Heeger, High-detectivity polymer photodetectors with spectral response from 300 nm to 1450 nm, *Science*, **2009**, *325*, 1665-1667.

6) G. Konstantatos, E. H. Sargent, Nanostructured materials for photon detection, *Nat. Nanotech*., **2010,** *5*, 391-400.

7) I, Moreels, Y. Justo, B. D. Geyter, M. K. Haustraete, Z. Hens, Z. Size-tunable, bright, and stable PbS quantum dots: a surface chemistry study, *ACS Nano*, **2011,** *5,* 2004-2012.

8) C. Giansante, I. Infante, E. Fabiano, R. Grisorio, G. P. Suranna, G. Gigli, "Darker-than-Black" PbS quantum dots: enhancing optical absorption of colloidal semiconductor nanocrystals via short conjugated ligands, *J. Am. Chem. Soc.,* **2015**, *137*, 1875-1886.

9) K. Qiao, H. Deng, X. Yang, D. Dong, M. Li, L. Hu, H. Liu, H. Song, J. Tang, Spectra-selective PbS quantum dot infrared photodetectors, *Nanoscale,* **2016**, *8*, 7137-7143.

10) F. W. Wise, Lead salt quantum dots: the limit of strong quantum confinement, *Acc. Chem. Res*., **2000,** *33,* 773-780.

11) F. Xia, T. Mueller, Y.-m. Lin, A. Valdes-Garcia, P. Avouris, Ultrafast graphene photodetector, *Nat. Nanotech.,* **2009**, *4*, 839-843.

12) C.-H. Liu, Y.-C. Chang, T. B. Norris, Z. Zhong, Graphene photodetectors with ultra-broadband and high responsivity at room temperature, *Nat. Nanotech.*, **2014**, *9*, 273-278.

13) K. Zhang, T. Zhang, G. Cheng, T. Li, S. Wang, W. Wei, X. Zhou, W. Yu, Y. Sun, P. Wang, D. Zhang, C. Zeng, X. Wang, W. Hu, H. J. Fan, G. Shen, X. Chen, X. Duan, K. Chang, N. Dai, Interlayer transition and IR photodetection in atomically thin type-II $MoTe_2/MoS_2$ van der Waals heterostructures, *ACS Nano,* **2016**, *10*, 3852-3858.

14) Y. Xie, B. Zhang, S. Wang, D. Wang, A. Wang, Z. Wang, H. Yu, H. Zhang, Y. Chen, M.

Zhao, B. Huang, L. Mei, J. Wang, Ultrabroadband MoS_2 photodetector with spectral response from 445 to 2717 nm, *Adv. Mater.,* **2017**, *29*, 1605972.

15) N. S. Sariciftci, L. Smilowitz, A. J. Heeger, F. Wudl, Photoinduced electron transfer from a conducting polymer to buckminsterfullerene, *Science*, **1992**, 1474-1476.

16) G. Yu, J. Gao, J. C. Hummelen, F. Wudl, A. J. Heeger, Polymer photovoltiac cells: Enhanced efficiencies via a network of internal donor-acceptor heterojunctions, *Science,* **1995,** *270*, 1789-1791.

17) L. Zheng, T. Zhu, W. Xu, L. Liu, J. Zheng, X. Gong, F. Wudl, Solution-processed broadband polymer photodetectors with a spectral response of up to 2.5 μm by a low bandgap donor–acceptor conjugated copolymer, *J. Mater. Chem. C,* **2018**, *6*, 3634-3641.

18) J. Han, J. Qi, X. Zheng, Y. Wang, L. Hu, C. Guo, Y. Wang, Y. Li, D. Ma, W. Qiao, Z. Y. Wang, Low-bandgap donor–acceptor polymers for photodetectors with photoresponsivity from 300 nm to 1600 nm, *J. Mater. Chem. C,* **2017**, *5*, 159-165.

19) L. Hu, J. Han, W. Qiao, X. Zhou, C. Wang, D. Ma, Y. Li, Z. Y. Wang, Side-chain engineering in naphthalenediimide-based n-type polymers for high-performance all-polymer photodetectors, *Polym. Chem.,* **2018**, *9*, 327-334.

20) L. Hu, W. Qiao, J. Han, X. Zhou, C. Wang, D. Ma, Z. Y. Wang, Y. Li, Naphthalene diimide–diketopyrrolopyrrole copolymers as non-fullerene acceptors for use in bulk-heterojunction all-polymer UV–NIR photodetectors, *Polym. Chem.,* **2017**, *8*, 528-536.

21) X. Wang, L. Lv, L. Li, Y. Chen, K. Zhang, H. Chen, H. Dong, J. Huang, G. Shen, Z. Yang, H. Huang, High-performance all-polymer photoresponse devices based on acceptor–acceptor conjugated polymers, *Adv. Funct. Mater.,* **2016**, *26*, 6306-6315.

22) H. Wang, S. Xing, Y. Zheng, J. Kong, J. Yu, A. D. Taylor, Three-phase morphology

evolution in sequentially solution-processed polymer photodetector: Toward low dark current and high photodetectivity, *ACS Appl. Mater. Interfaces,* **2018**, *10*, 3856-3864.

23) X. Hu, K. Wang, C. Liu, T. Meng, Y. Dong, S. Liu, F. Huang, X. Gong, Y. Cao, High-detectivity inverted near-infrared polymer photodetectors using cross-linkable conjugated polyfluorene as an electron extraction layer, *J. Mater. Chem. C,* **2014**, *2*, 9592-9598.

24) X. Liu, J. Zhou, J. Zheng, M. L. Becker, X. Gong, Water-soluble CdTe quantum dots as an anode interlayer for solution-processed near infrared polymer photodetectors, *Nanoscale,* **2013**, *5*, 12474-12479.

25) L. Zhang, T. Yang, L. Shen, Y. Fang, L. Dang, N. Zhou, X. Guo, Z. Hong, Y. Yang, H. Wu, J. Huang, Y. Liang, Toward highly sensitive polymer photodetectors by molecular engineering, *Adv. Mater.,* **2015**, *27*, 6496-6503.

26) W. Wang, F. Zhang, L. Li, M. Gao, B. Hu, Improved performance of photomultiplication polymer photodetectors by adjustment of P3HT molecular arrangement, *ACS Appl. Mater. Interfaces,* **2015**, *7*, 22660-22668.

27) L. L. Li, F. J. Zhang, W, B, Wang, Q. S. An, J. Wang, Q. Q. Sun, M. Zhang, Trap-assisted photomultiplication polymer photodetectors obtaining an external quantum efficiency of 37 500%, ACS *Appl. Mater. Interfaces,* **2015**, 7, 10, 5890–5897

28) K. X. Yang, J. Wang, Z. J. Zhao, Z. J. Zhou, M. Liu, J. Zhang, Z. Q. He, F. J. Zhang, Smart strategy: transparent hole-transporting polymer as a regulator to optimize photomultiplication-type polymer photodetectors, *ACS Appl. Mater. Interfaces,* **2021**, 13, 21565.

29) Z. J. Zhao, M. Liu, K. X. Yang, C. Y. Xu, Y. X. Guan, X. L. Ma, J. Wang, F. J. Zhang, Highly sensitive narrowband photomultiplication-type organic photodetectors prepared by

transfer-Printed technology, Adv. Funct. Mater. 2021, 2106009

30) V. V. Diev, K. Hanson, J. D. Zimmerman, S. R. Forrest, M. E. Thompson, Fused pyrene-diporphyrins: shifting near-infrared absorption to 1.5 μm and beyond, *Angew. Chem. Int. Ed.,* **2010**, *49*, 5523-5526.

31) E. Bundgaard, F. C. Krebs, Low band gap polymers for organic photovoltaics, *Sol. Energy. Mater. Sol. Cells,* **2007**, *91*, 954-985.

32) E. Perzon, F. Zhang, M. Andersson, W. Mammo, O. Inganäs, M. R. Andersson, A conjugated polymer for near-infrared optoelectronic applications, *Adv. Mater.,* **2007**, *19*, 3308-3311.

33) G. Konstantatos, J. Clifford, L. Levina, E. H. Sargent, Sensitive solution-processed visible-wavelength photodetectors, *Nat. Photonics,* **2007**, *1*, 531-534.

34) G. Konstantatos, I. Howard, A. Fischer, S. Hoogland, J. Clifford, E. Klem, L. Levina, E. H. Sargent, Ultrasensitive solution-cast quantum dot photodetectors, *Nature,* **2006**, *442*, 180-183.

35) C. Liu, K. Wang, C. Yi, X. Shi, P. Du, A. W. Smith, A. Karim, X. Gong, Ultrasensitive solution-processed perovskite hybrid photodetectors, *J. Mater. Chem. C,* **2015**, *3*, 6600-6606.

36) C. Liu, K. Wang, P. Du, E. Wang, X. Gong, A. J. Heeger, Ultrasensitive solution-processed broad-band photodetectors using $CH_3NH_3PbI_3$ perovskite hybrids and PbS quantum dots as light harvesters, *Nanoscale,* **2015**, *7*, 16460-16469.

37) C. Liu, K. Wang, X. Gong, A. J. Heeger, Low bandgap semiconducting polymers for polymeric photovoltaics, *Chem. Soc. Rev.,* **2016**, *45*, 4825-4846.

38) C. Liu, H. Peng, K. Wang, C. Wei, Z. Wang, X. Gong, PbS quantum dots-induced trap-

assisted charge injection in perovskite photodetectors, *Nano Energy,* **2016**, *30*, 27-35.

39) W. Xu, H. Peng, T. Zhu, C. Yi, L. Liu, X. Gong, A solution-processed near-infrared polymer: PbS quantum dot photodetectors, *RSC Adv.,* **2017**, *7*, 34633-34637.

40) L. Zheng, T. Zhu, W. Xu, J. Zheng, L. Liu, X. Gong, Ultrasensitive perovskite photodetectors by Co partially substituted hybrid perovskite, *ACS Sustain. Chem. Eng.,* **2018**, *6*, 12055-12060.

41) T. Zhu, L. Zheng, X. Yao, L. Liu, F. Huang, Y. Cao, X. Gong, Ultrasensitive solution-processed broadband PbSe photodetectors through photomultiplication effect, *ACS Appl. Mater. Interfaces,* **2019**, *11*, 9205-9212.

42) T. Zhu, Y. Yang, L. Zheng, L. Liu, M. L. Becker, X. Gong, Solution-processed flexible broadband photodetectors with solution-processed transparent polymeric electrode, *Adv. Funct. Mater*., **2020**, *30*, 1909487.

43) B. D. Gates, Flexible electronics, *Science*, **2009,** 323, 1566-1567.

44) D. Alemu, H.-Y. Wei, K.-C. Ho, C.-W. Chu, Highly conductive PEDOT:PSS electrode by simple film treatment with methanol for ITO-free polymer solar cells, *Energy Environ. Sci.,* **2012**, *5*, 9662-9671.

45) X. Mei, J. Ouyang, Highly conductive and transparent single-walled carbon nanotube thin films fabricated by gel coating, *J. Mater. Chem.,* **2011**, *21*, 17842-17849.

46) J. Du, S. Pei, L. Ma, H. M. Cheng, 25th Anniversary article: Carbon nanotube- and graphene-based transparent conductive films for optoelectronic devices, *Adv. Mater.,* **2014**, *26,* 1958-1991.

47) Z. Yu, Q. Zhang, L. Li, Q. Chen, X. Niu, J. Liu, Q. Pei, Highly flexible silver nanowire electrodes for shape-memory polymer light-emitting diodes, *Adv. Mater.* **2011**, *23,* 664-668.

48) Y. Xia, K. Sun, J. Ouyang, Solution-processed metallic conducting polymer films as transparent electrode of optoelectronic devices, *Adv. Mater.,* **2012**, *24,* 2436-2440.

49) Y. Xia, K. Sun, J. Ouyang, Highly conductive poly(3,4-ethylenedioxythiophene):poly(styrene sulfonate) films treated with an amphiphilic fluoro compound as the transparent electrode of polymer solar cells, *Energy Environ. Sci.,* **2012**, *5*, 5325-5332.

50) M. Vosgueritchian, D. J. Lipomi, Z. Bao, Highly conductive and transparent PEDOT:PSS films with a fluorosurfactant for stretchable and flexible transparent electrodes, *Adv. Funct. Mater.,* **2012**, *22,* 421-428.

51) J. Ouyang, Solution-processed PEDOT:PSS films with conductivities as indium tin oxide through a treatment with mild and weak organic acids, *ACS Appl. Mater. Interfaces,* **2013**, *5,* 13082-13088.

52) M. Sykora, A. Y. Koposov, J. A. McGuire, R. K. Schulze, O. Tretiak, J. M. Pietryga, V. I. Klimov, Effect of air exposure on surface properties, electronic structure, and carrier relaxation in PbSe nanocrystals, *ACS Nano,* **2010**, *4*, 2021-2034.

53) D. K. Kim, Y. Lai, B. T. Diroll, C. B. Murray, C. R. Kagan, Flexible and low-voltage integrated circuits constructed from high-performance nanocrystal transistors, *Nat. Commun.,* **2012**, *3*, 1216.

54) A. Nag, M. V. Kovalenko, J.-S. Lee, W. Liu, B. Spokoyny, D. V. Talapin, Metal-free inorganic ligands for colloidal nanocrystals: S^{2-}, HS^{-}, Se^{2-}, HSe^{-}, Te^{2-}, HTe^{-}, TeS_3^{2-}, OH^{-}, and NH^{2-} as surface ligands, *J. Am. Chem. Soc.,* **2011,** *133,* 10612-10620.

55) A. T. Fafarman, W.-k. Koh, B. T. Diroll, D. K. Kim, D.-K. Ko, S. J. Oh, X. Ye, V. Doan-Nguyen, M. R. Crump, D. C. Reifsnyder, C. B. Murray, C. R. Kagan, Thiocyanate-capped

nanocrystal colloids: vibrational reporter of surface chemistry and solution-based route to enhanced coupling in nanocrystal solids, *J. Am. Chem. Soc*., **2011,** *133,* 15753-15761.

56) T. Takagahara, K. Takeda, Theory of the quantum confinement effect on excitons in quantum dots of indirect-gap materials, *Phys. Rev. B,* **1992**, *46*, 15578-15581.

57) H. Dong, H. Zhu, Q. Meng, X. Gong, W. Hu, Organic photoresponse materials and devices, *Chem. Soc. Rev*., **2012**, *41*, 1754-1808.

58) Y. Xia, L. Wang, X. Deng, D. Li, X. Zhu, Y. Cao, Photocurrent response wavelength up to 1.1μm from photovoltaic cells based on narrow-band-gap conjugated polymer and fullerene derivative, *Appl. Phys. Lett.,* **2006**, *89*, 081106.

59) T. Erb, U. Zhokhavets, G. Gobsch, S. Raleva, B. Stühn, P. Schilinsky, C. Waldauf, C. J. Brabec, Correlation between structural and optical properties of composite polymer/fullerene films for organic solar cells, *Adv. Funct. Mater.,* **2005**, *15*, 1193-1196.

60) H. Krüger, E. Kemnitz, A. Hertwig, U. Beck, Transparent MgF_2-films by sol-gel coating: Synthesis and optical properties, *Thin Solid Films*, **2008**, *516*, 4175-4177.

61) D. W. Steuerman, A. Garcia, M. Dante, R. Yang, J. P. Löfvander, T.-Q. Nguyen, Imaging the interfaces of conjugated polymer optoelectronic devices, *Adv. Mater.*, **2008**, *20*, 528-534.

62) D. R. Rainer, C. Xu, P. M. Holmblad, D. W. Goodman, Pd, Cu, and Au particles on Al_2O_3 thin films: an infrared reflection absorption spectroscopy study of monometallic and bimetallic planar model supported catalysts, *J. Vac. Sci. Technol. A*, **1997**, *15*, 1653-1662.

63) S. R. Cowan, A. Roy, A. J. Heeger, Recombination in polymer-fullerene bulk heterojunction solar cells, *Phys. Rev. B,* **2010**, *82*, 245207.

64) J. L. Bredas, G. B. Street, Polarons, bipolarons, and solitons in conducting polymers, *Acc. Chem. Res.,* **1985**, *18*, 309–315.

65) C. Deibel, T. Strobel, V. Dyakonov, Origin of the efficient polaron-pair dissociation in polymer-fullerene blends, *Phys. Rev. Lett.,* **2009**, *103*, 036402.

66) S. M. Sze, K. K. Ng, Physics of Semiconductor Devices, 3rd Ed John Wiley & Sons, Inc. 2006.

67) Y. Wang, D. Yang, X. Zhou, D. Ma, A. Vadim, T. Ahamad, S. M. Alshehri, Perovskite/Polymer hybrid thin films for high external quantum efficiency photodetectors with wide spectral response from visible to near-infrared wavelengths, *Adv. Optical Mater.,* **2017**, *5*, 1700213.

68) W. Xu, Y. Guo, X. Zhang, L. Zheng, T. Zhu, D. Zhao, W. Hu, X. Gong, Room-temperature-operated ultrasensitive broadband photodetectors by perovskite incorporated with conjugated polymer and single-wall carbon nanotubes, *Adv. Funct. Mater.,* **2018**, *28*, 1705541.

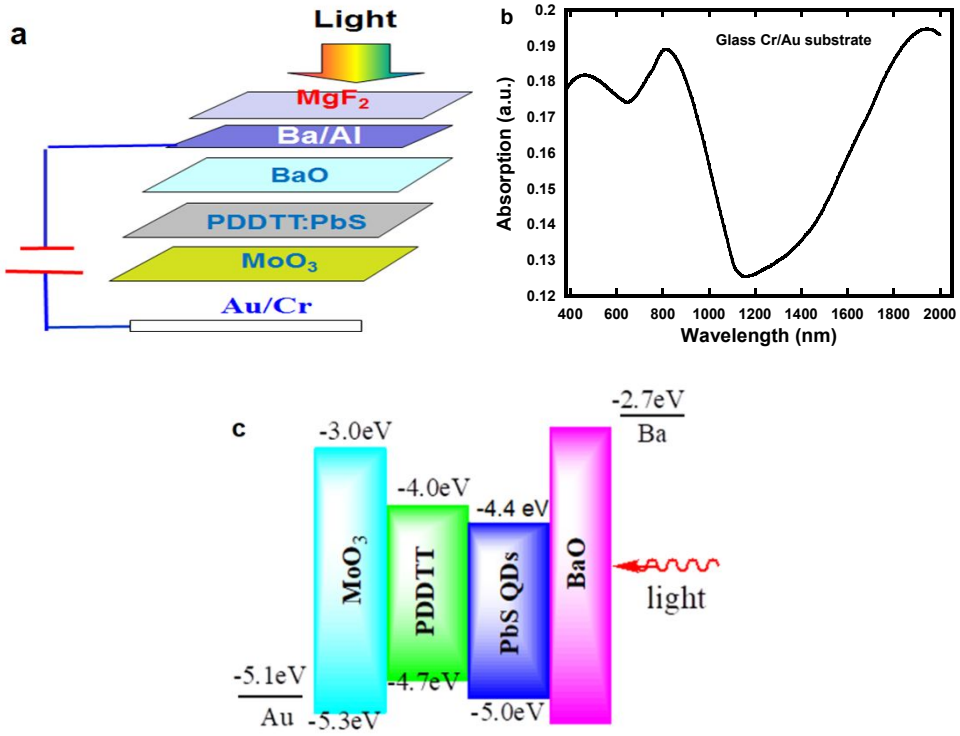

Scheme 1. (a) Device architecture of broadband photodetectors, (b) the absorption spectrum of glass Cr/Au thin film, and (c) the LUMO and HOMO energy levels of MoO_3, PDDTT, PbS QDs, BaO, and the work functions of Au and Ba electrodes.

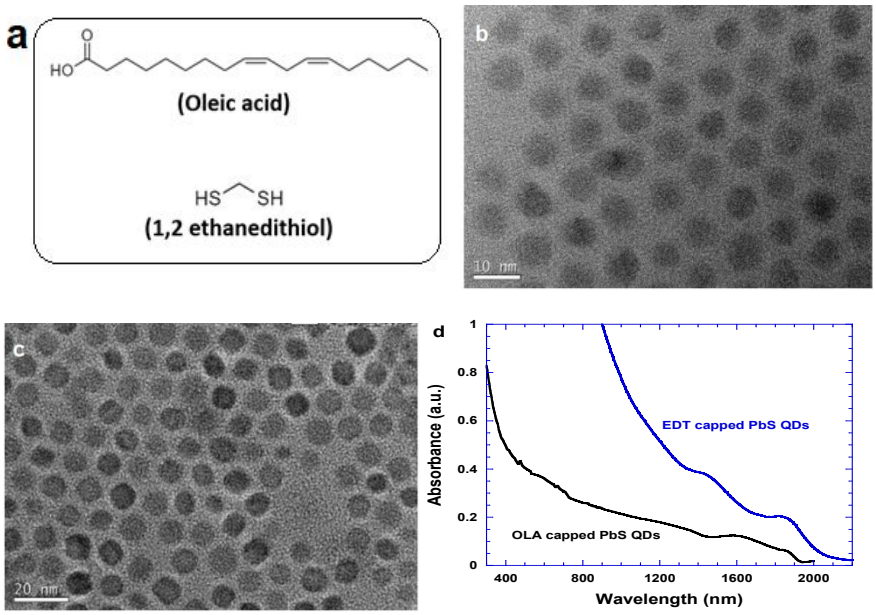

Figure 1. (a) Molecular structures of OLA and EDT, the TEM images of (b) the OLA capped PbS QDs thin film and (c) the EDT capped PbS QDs thin film, and (d) absorption spectra of two different PbS QDs thin films.

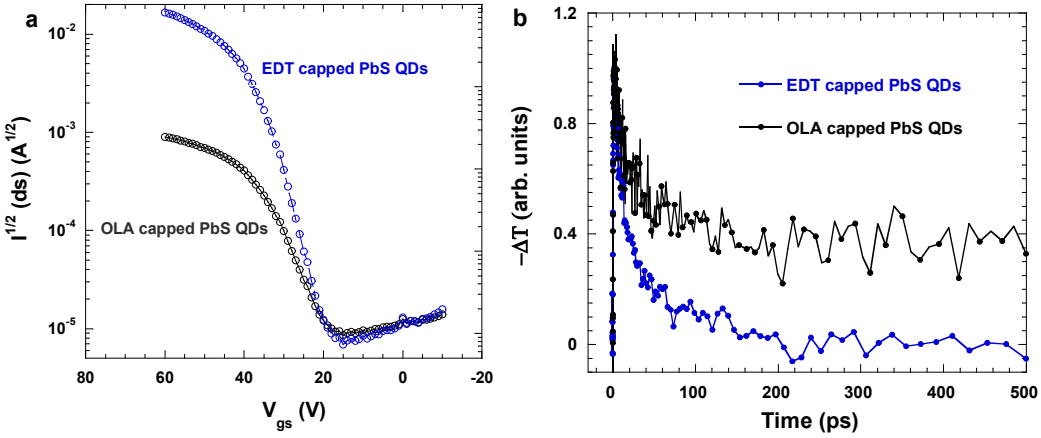

Figure 2. (a) The I_{DS} versus V_G characteristics of thin film transistors based on PbS QDs thin films, (b) the transient decay dynamics of PbS QDs thin films probed at 4.7 mm.

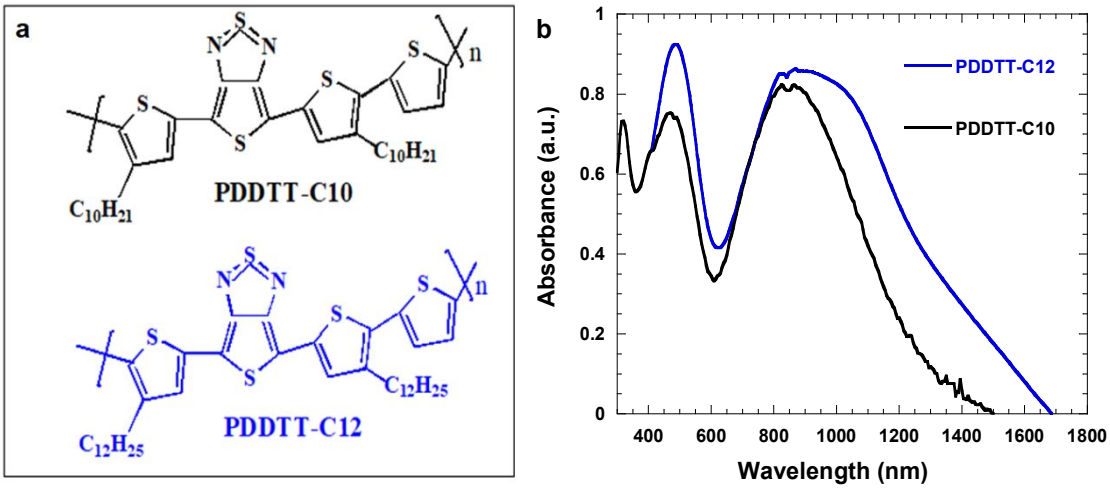

Figure 3. (a) Molecular structures and (b) absorption spectra of PDDTT with different side chains.

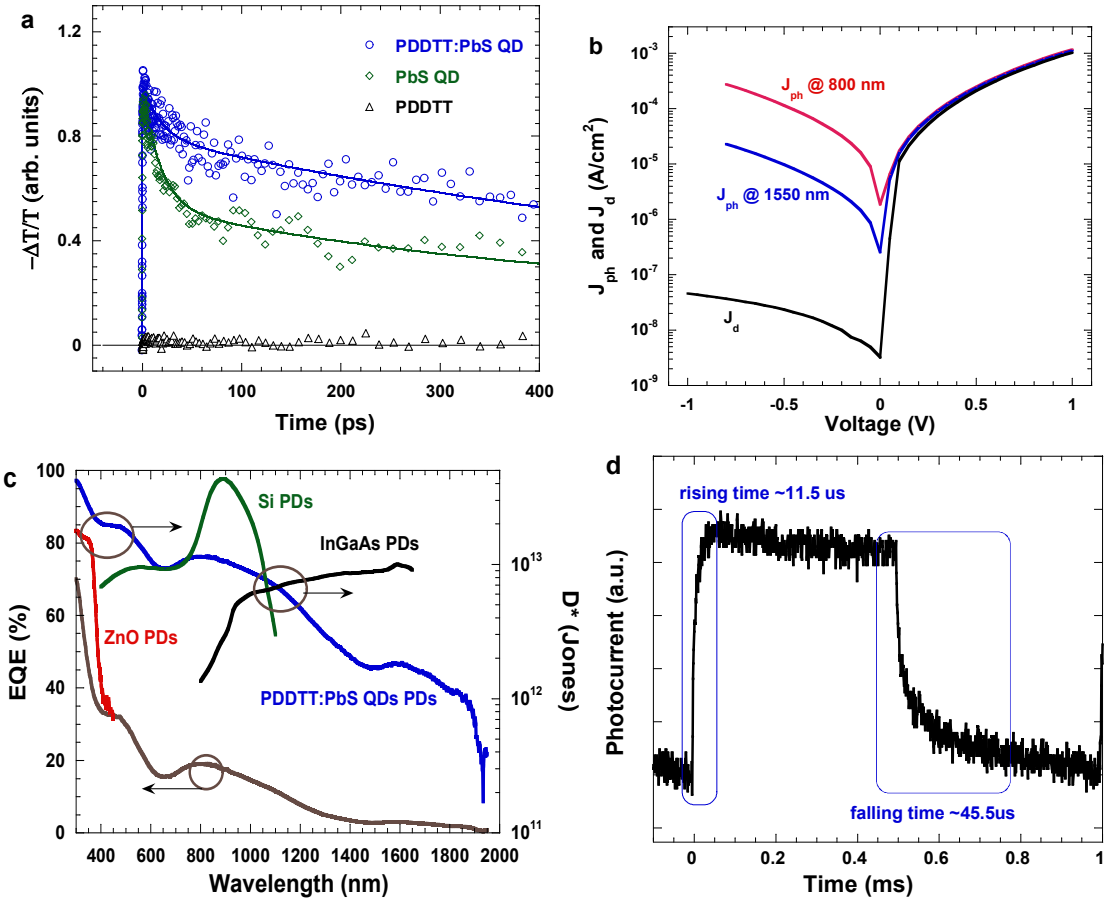

Figure 4. (a) The transient decay dynamics of PDDTT and PbS QDs thin films and PDDTT:PbS QDs BHJ composite thin film, (b) the J-V characteristics of broadband PDs, (c) the EQE spectrum of the broadband PDs and the projected detectivities of the broadband PDs versus wavelength, compared with ZnO based PDs, Si-based PDs and InGaAs based PDs, and (d) the photocurrent response time of broadband PDs.